Mendeleev Communications

Mendeleev Commun., 2025, **35**, 169–171

Polyfluorinated Blatter radicals

Dmitry A. Gulyaev,[a] Nurlan V. Gadimov,[a,b] Nina P. Gritsan,[c] Evgeny M. Kadilenko,[c] Pavel G. Shangin,[a] Mikhail A. Syroeshkin,[a] Egor A. Sosunov[b,d] and Evgeny V. Tretyakov*[a]

[a] *N. D. Zelinsky Institute of Organic Chemistry, Russian Academy of Sciences, 119991 Moscow, Russian Federation. E-mail: tretyakov@ioc.ac.ru*
[b] *D. Mendeleev University of Chemical Technology of Russia, 125047 Moscow, Russian Federation*
[c] *V. V. Voevodsky Institute of Chemical Kinetics and Combustion, Siberian Branch of the Russian Academy of Sciences, 630090 Novosibirsk, Russian Federation*
[d] *N. S. Kurnakov Institute of General and Inorganic Chemistry, Russian Academy of Sciences, 119991 Moscow, Russian Federation*

DOI: 10.71267/mencom.7724

The first benzotriazinyl radicals containing fluorine atoms in both aryl substituents were synthesized from polyfluorophenylhydrazines and 4-fluoro-*N*-phenylbenzimidoyl chloride. Their crystal structure and magnetic properties were studied thus revealing strong antiferromagnetic interactions (J/k_B from –160 to –185 K).

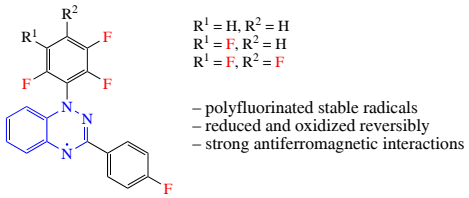

Keywords: organofluorine compounds, heterocycles, organic radicals, 1,2,4-benzotriazin-4-yls, magnetostructural correlations.

The exploration of open-shell compounds has sparked considerable interest and become a broadly investigated subject.[1–4] New approaches to their synthesis and stabilization led to a wide variety of radicals with lifetime sufficient for many applications. Among them, there are 1,4-dihydro-1,2,4-benzotriazin-4-yl radicals known as Blatter radicals.[5,6] Due to their stability, Blatter radicals are used in molecular grafting and design,[7] spintronics and electronics,[8,9] as polymerization initiators,[10,11] photodetectors,[12] qubits for quantum computing,[13] and for the production of liquid crystals.[14,15]

In our previous studies, we have found that the presence of fluorine atoms in the arene part of the triazinyl core substantially affected the packing of Blatter radicals and their magnetic properties.[16,17] To expand the structural diversity of fluorinated 1,2,4-benzotriazinyl radicals and to shed light on their inherent structure–property correlations, we report the synthesis and complete characterization of benzotriazinyl radicals containing F atoms in both phenyl substituents, namely 1-(2,3,6-trifluorophenyl)- (**1a**), 1-(2,3,5,6-tetrafluorophenyl)- (**1b**), and 1-(2,3,4,5,6-pentafluorophenyl)-3-(4-fluorophenyl)-1,4-dihydro-1,2,4-benzotriazin-4-yl (**1c**).

The syntheses of radicals **1a–c** involved *in situ* oxidation of the corresponding amidrazones giving 1,2,4-triazabutadienes, which were then subjected to electrocyclic ring closure to form benzotriazines, which were next oxidized to the target products (Scheme 1).[18–21] Chemically pure samples of 1,2,4-benzotriazinyl radicals **1a–c** were obtained by column chromatography on silica gel followed by recrystallization from a mixture of CH_2Cl_2 with *n*-hexane. The obtained radicals were comprehensively studied in solution and in the solid state.

Voltammetric curves of compounds **1a–c** obtained in MeCN and DMF are shown in Figures 1 and S6–S11 (see Online Supplementary Materials); potentials are summarized in Table 1. All the compounds are reduced and oxidized reversibly in both media with peak potential differences of 63–69 mV, which is very close to the theoretical value for a fully reversible process (59 mV).[21] Considering the acceptor nature of fluorine, one would expect a decrease in reduction potentials and an increase in oxidation potentials in the series **1a–c**. Indeed, the corresponding values $E^{red}_{1/2}$ for **1a–c** are –954, –896, and –888 mV in MeCN and –952, –934, and –885 mV in DMF.

Oxidation potentials $E^{ox}_{1/2}$ in the series **1a–c** are even less sensitive to the increase in the number of fluorine atoms in the 1-aryl substituent; the corresponding values are 231, 270, and 278 mV in MeCN and 240, 234, and 275 mV in DMF. Thus, the observed change in redox potentials is rather small, and the solvent has almost no effect on them.

Continuous-wave ESR spectra of 1,2,4-benzotriazinyls **1a–c** were recorded at room temperature in degassed toluene solutions. All spectra consist of seven-line multiplets resulting from

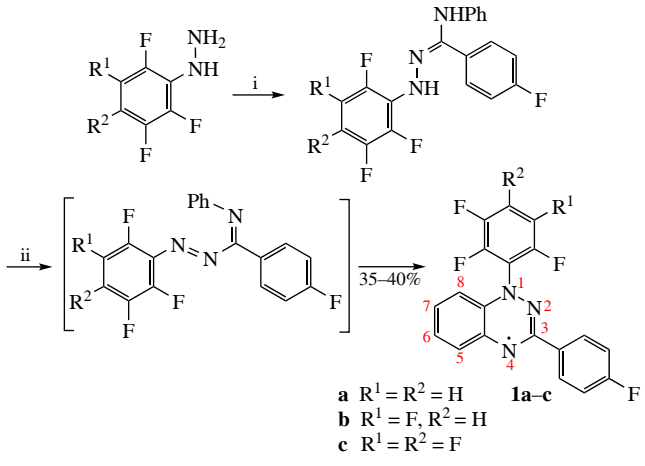

Scheme 1 *Reagents and conditions*: i: 4-fluoro-*N*-phenylbenzimidoyl chloride, Et_3N, THF, 24 h, room temperature; ii: MnO_2, CH_2Cl_2, 6–30 h, room temperature.

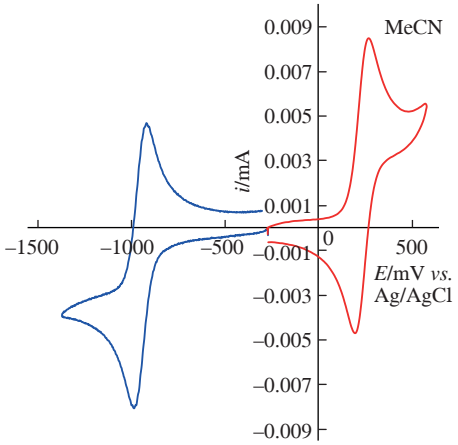

Figure 1 Cyclic voltammetry curves of oxidation and reduction of **1a** (1×10^{-3} M) in 0.1 M Bu_4NBF_4/MeCN on a glassy carbon disk electrode at a potential sweep rate of 0.1 V s^{-1}.

Table 1 Potentials of forward (fw) and reverse (rev) peaks of the volt-ampere reduction (red) and oxidation (ox) curves and half-wave potentials for compounds **1a–c**.

Radical	Solvent	$E^{p,red}_{fw}$	$E^{p,red}_{rev}$	$E^{red}_{1/2}$	$E^{p,ox}_{fw}$	$E^{p,ox}_{rev}$	$E^{ox}_{1/2}$
1a[a]	MeCN	–989[b]	–920[c]	–954	263	199	231
	DMF	–984	–919	–952	274	207	240
1b	MeCN	–929	–862	–896	303	236	270
	DMF	–967	–900	–934	267	200	234
1c	MeCN	–919	–856	–888	312	245	278
	DMF	–918	–852	–885	308	242	275

[a] Cyclic voltammetry curves were registered on a glass-carbon electrode in 0.1 M Bu_4NPF_6/MeCN and DMF. [b] All values are in mV relative to Ag/AgCl. [c] Values of potentials were obtained by extrapolating the 'peak potential–peak current' dependencies to the zero current for curves recorded at 25, 50, 100, 200, 500, and 1000 mV s^{-1}.

hyperfine interactions between an unpaired electron and three similar but slightly nonequivalent ^{14}N nuclei (Figures 2, S12 and S13). For **1a**, hyperfine coupling (HFC) constants and g_{iso}, determined *via* modeling of EPR spectrum and calculated at the UB3LYP/def2-QZVP level, are $a_{N(1)} = 0.69/0.52$, $a_{N(2)} = 0.52/0.46$, and $a_{N(4)} = 0.55/0.50$ mT with $g = 2.0040/2.0034$. A comparison of the calculated HFC constants and Mulliken spin populations of the N atoms (Figure S15) showed that they do not correlate, which can be explained by a small deviation from the planarity of the triazinyl ring. This deviation leads to a small difference in the hybridization of the N atoms and consequently in the populations of their s-type atomic orbitals.

Single crystals of radicals **1a–c** were grown by slow evaporation of their solutions in a mixture of *n*-hexane with

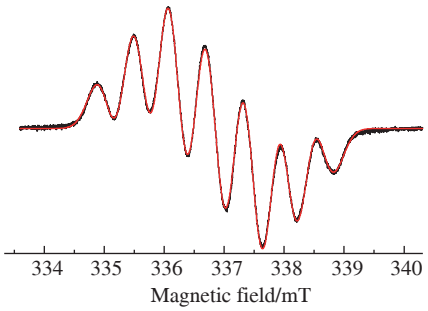

Figure 2 Experimental (black) and simulated (red) ESR spectra for a degassed ~10^{-5} M solution of **1a** in toluene at 298 K.

CH_2Cl_2. X-ray diffraction revealed that radicals **1a**, **1b**, and **1c** crystallized in monoclinic space groups *Pc* and $P2_1$ and triclinic space group $P\bar{1}$, respectively (Figure 3, Table S1 in Online Supplementary Materials).† Selected bond lengths, contacts, and torsion angles in **1a–c** are summarized in Table S2.

In the structure of both **1a** and **1b**, four crystallographically independent molecules are similar in bond lengths; they differ in the angle of rotation of the plane of the tri- or tetrafluorophenyl ring relative to the bicycle plane. As for the monofluorinated rings, they lie almost in the plane of the heterocyclic nucleus (Table S2). The asymmetric unit of **1c** contains two crystallographically independent molecules also differing in the angle of rotation of the plane of the pentafluorophenyl ring toward the heterocyclic plane.

According to the data of XRD analysis, crystals of **1a–c** have a network of short contacts (less than the sum of van der Waals radii) of C–H···F, F···F, and C···C types (Figures S3–S5, Table S2). As the number of fluorine atoms increases, there is a tendency for a decrease in the length of respective contacts, and

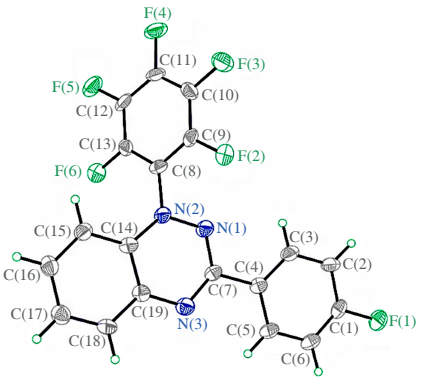

Figure 3 An ORTEP diagram of polyfluorinated radical **1c** at the 50% probability level and a crystallographic numbering scheme of selected nonhydrogen atoms.

† *Crystal data for* **1a**. $C_{19}H_{10}F_4N_3$ ($M = 356.30$), monoclinic, $a = 7.6749(9)$, $b = 13.2865(15)$ and $c = 29.611(3)$ Å, $\beta = 96.469(4)°$, $V = 3000.3(6)$ Å^3, space group *Pc*, $Z = 8$, $d_{calc} = 1.578$ g cm^{-3}, $F(000) = 1448$, $\mu = 0.131$ mm^{-1}. A total of 30753 reflections (9337 unique, $R_{int} = 0.0884$) were measured with a Bruker D8 Venture diffractometer (graphite monochromatized MoKα radiation, $\lambda = 0.71073$ Å) using ω- and φ-scan modes at 100(2) K. The final residuals were $R_1 = 0.0657$ for 6583 reflections with $I > 2\sigma(I)$ and $wR_2 = 0.1688$ for all data and 967 parameters. GoF = 1.065.

Crystal data for **1b**. $C_{19}H_9F_5N_3$ ($M = 374.29$), monoclinic, $a = 7.72710(10)$, $b = 29.9761(5)$ and $c = 13.2726(2)$ Å, $\beta = 91.0326(9)°$, $V = 3073.81(8)$ Å^3, space group $P2_1$, $Z = 8$, $d_{calc} = 1.618$ g cm^{-3}, $F(000) = 1512$, $\mu = 1.229$ mm^{-1}. A total of 38954 reflections (11522 unique, $R_{int} = 0.0815$) were measured with a Bruker D8 Venture diffractometer (graphite monochromatized CuKα radiation, $\lambda = 1.54178$ Å) using ω- and φ-scan modes at 200(2) K. The final residuals were $R_1 = 0.0575$ for 9737 reflections with $I > 2\sigma(I)$ and $wR_2 = 0.1690$ for all data and 974 parameters. GoF = 1.043.

Crystal data for **1c**. $C_{19}H_8F_6N_3$ ($M = 392.28$), triclinic, $a = 7.5444(4)$, $b = 13.4606(5)$ and $c = 15.7307(8)$ Å, $\alpha = 102.175(2)°$, $\beta = 96.784(3)°$, $\gamma = 91.454(3)°$, $V = 1548.54(13)$ Å^3, space group $P\bar{1}$, $Z = 4$, $d_{calc} = 1.683$ g cm^{-3}, $F(000) = 788$, $\mu = 0.153$ mm^{-1}. A total of 5508 reflections (5508 unique, $R_{int} = 0.0637$) were measured with a Bruker D8 Venture diffractometer (graphite monochromatized MoKα radiation, $\lambda = 0.71073$ Å) using ω- and φ-scan modes at 100(2) K. The final residuals were $R_1 = 0.0601$ for 3027 reflections with $I > 2\sigma(I)$ and $wR_2 = 0.1477$ for all data and 506 parameters. GoF = 0.993.

CCDC 2407367, 2407368, and 2407369 contain the supplementary crystallographic data for this paper. These data can be obtained free of charge from The Cambridge Crystallographic Data Centre *via* https://www.ccdc.cam.ac.uk.

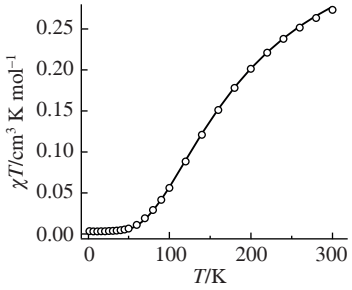

Figure 4 The temperature dependence of the χT product for radical **1b** (open circles). The solid curve is a simulation for a magnetic motif consisting of a fraction of non-interacting radicals (p) and a fraction of radicals forming two types of antiferromagnetically coupled dimers.

the calculated crystal density increases from 1.578 g cm^{-3} in **1a** to 1.618 g cm^{-3} in **1b** and 1.683 g cm^{-3} in **1c**. Overall, a tendency of crystal density to increase was observed in the series starting from 1,3-diphenyl-1,4-dihydro-1,2,4-benzotriazin-4-yl as fluorine atoms are introduced into the phenyl substituents, reaching a maximum value in **1c**.

Temperature dependences of χT for radicals **1a–c** are shown in Figures 4, S20, and S21. For **1b**, χT at 300 K is 0.277 cm^3 K mol^{-1} and diminishes with lowering of the temperature, reaching a plateau of ~0.003 cm^3 K mol^{-1} below 50 K.

The high-temperature value of χT is well below the theoretical spin-only value of 0.375 cm^3 K mol^{-1} for noninteracting radicals at $g = 2$, indicating strong antiferromagnetic exchange interactions; the latter result is consistent with our BS-DFT calculations (Table S4). We simulated the dependence of χT on T for **1b** using a magnetic motif consisting of two types of antiferromagnetically coupled dimers. The following parameters correspond to the best fit: $J_1/k_B = -185 \pm 3$ K, $J_2/k_B = -152 \pm 2$ K, $g = 2.11 \pm 0.01$, $p = 0.009$. Note that the values of J_1 and J_2 are consistent with the calculations (–243 and –173 K).

Online Supplementary Materials

Supplementary data associated with this article can be found in the online version at doi: 10.71267/mencom.7724.

References

1 E. Tretyakov, in *Organic Radicals,* eds. C. Wang, A. Labidi and E. Lichtfouse, Elsevier, Amsterdam, 2024, ch. 5, pp. 61–181; https://doi.org/10.1016/B978-0-443-13346-6.00005-1.
2 Z. X. Chen, Y. Li and F. Huang, *Chem*, 2021, **7**, 288; https://doi.org/10.1016/j.chempr.2020.09.024.
3 *Stable Radicals: Fundamentals and Applied Aspects of Odd-Electron Compounds*, ed. R. G. Hicks, John Wiley & Sons, Chichester, 2010; https://doi.org/10.1002/9780470666975.
4 A. A. Buravlev, A. Yu. Makarov, O. A. Rakitin and A. V. Zibarev, *Mendeleev Commun.*, 2023, **33**, 439; https://doi.org/10.1016/j.mencom.2023.06.001.
5 J. M. Rogers, P. L. Norcott and M. L. Coote, *Org. Biomol. Chem*., 2020, **18**, 8255; https://doi.org/10.1039/D0OB01394C.
6 G. M. Ziarani, M. Mostofi, P. Gholamzadeh, M. Mohammadi-Khanaposhtani and H. Yavari, *ARKIVOC*, 2019, **(i)**, 41; https://doi.org/10.24820/ark.5550190.p010.791.
7 S. Kapuściński, B. Anand, P. Bartos, J. M. Garcia Fernandez and P. Kaszyński, *Molecules*, 2022, **27**, 1176; https://doi.org/10.3390/molecules27041176.
8 A. Calzolari, A. Rajca and M. B. Casu, *J. Mater. Chem. C*, 2021, **9**, 10787; https://doi.org/10.1039/D1TC01541A.
9 Y. Zhang, Y. Zheng, H. Zhou, M.-S. Miao, F. Wudl and T.-Q. Nguyen, *Adv. Mater*., 2015, **27**, 7412; https://doi.org/10.1002/adma.201502404.
10 J. Areephong, K. M. Mattson, N. J. Treat, S. O. Poelma, J. W. Kramer, H. A. Sprafke, A. A. Latimer, J. Read de Alaniz and C. J. Hawker, *Polym. Chem*., 2016, **7**, 370; https://doi.org/10.1039/C5PY01563D.
11 M. Demetriou, A. A. Berezin, P. A. Koutentis and T. Krasia-Christoforou, *Polym. Int*., 2014, **63**, 674; https://doi.org/10.1002/pi.4566.
12 Y. Zheng, M.-S. Miao, G. Dantelle, N. D. Eisenmenger, G. Wu, I. Yavuz, M. L. Chabinyc, K. N. Houk and F. Wudl, *Adv. Mater*., 2015, **27**, 1718; https://doi.org/10.1002/adma.201405093.
13 A. S. Poryvaev, E. Gjuzi, D. M. Polyukhov, F. Hoffmann, M. Fröba and M. V. Fedin, *Angew. Chem., Int. Ed*., 2021, **60**, 8683; https://doi.org/10.1002/anie.202015058.
14 P. Kaszyński, S. Kapuściński and S. Ciastek-Iskrzycka, *Adv. Heterocycl. Chem*., 2019, **128**, 263; https://doi.org/10.1016/bs.aihch.2019.01.001.
15 M. Jasiński, J. Szczytko, D. Pociecha, H. Monobe and P. Kaszyński, *J. Am. Chem. Soc.*, 2016, **138**, 942; https://doi.org/10.1021/jacs.6b06444.
16 D. Gulyaev, A. Serykh, E. Tretyakov, A. Akyeva, M. Syroeshkin, D. E. Gorbunov, S. V. Maltseva, N. P. Gritsan, G. Romanenko and A. Bogomyakov, *Catalysts*, 2023, **13**, 1206; https://doi.org/10.3390/catal13081206.
17 D. Gulyaev, A. Serykh, D. Gorbunov, N. Gritsan, A. Akyeva, M. Syroeshkin, G. Romanenko and E. Tretyakov, *Cryst. Growth Des.*, 2024, **24**, 5764; https://doi.org/10.1021/acs.cgd.4c00537.
18 L. L. Fershtat, *Chem. Heterocycl. Compd.*, 2022, **58**, 196; https://doi.org/10.1007/s10593-022-03072-z.
19 R. F. Fatykhov, I. A. Khalymbadzha, A. D. Sharapov, A. P. Potapova, E. S. Starnovskaya, D. S. Kopchuk and O. N. Chupakhin, *Chim. Techno Acta*, 2023, **10**, 2202310205; https://doi.org/10.15826/chimtech.2023.10.2.05.
20 J. A. Grant, Z. Lu, D. E. Tucker, B. M. Hockin, D. S. Yufit, M. A. Fox, R. Kataky, V. Chechik and A. C. O'Donoghue, *Nat. Commun*., 2017, **8**, 15088; https://doi.org/10.1038/ncomms15088.
21 Y. Ji, L. Long and Y. Zheng, *Mater. Chem. Front*., 2020, **4**, 3433; https://doi.org/10.1039/D0QM00122H.
22 A. J. Bard and L. R. Faulkner, *Electrochemical Methods: Fundamentals and Applications*, 2nd edn., Wiley, New York, 2001; https://archive.org/details/allen-j-bard-larry-r-faulkner-1-electrochemistry/mode/2up.
23 A. J. Bard and L. R. Faulkner, *Russ. J. Electrochem*., 2002, **38**, 1364; https://doi.org/10.1023/A:1021637209564.

Received: 14th January 2025; Com. 25/7724